ACS OMEGA

Open Access

http://pubs.acs.org/journal/acsodf

Article

Study on Electrochemical Behaviors of Heat-Treated *Escherichia coli* and *Staphylococcus aureus*

Xiaofan Wu, Yupo He, Jiaqi Fu, and Yanli Zhao*

Cite This: *ACS Omega* 2024, 9, 44907−44915

Read Online

ACCESS | Metrics & More | Article Recommendations | Supporting Information

ABSTRACT: Evaluating the bacterial activity effectively is critical to addressing the challenges posed by bacterial infections. Electrochemistry offers significant advantages in accuracy and cost efficiency compared with methods that are more time-consuming or require expensive instrumentation. This study initially established an electrochemical method for detecting bacterial activity using heat treatment as the pretreatment step. Subsequent optimization of the heat treatment and detection conditions further enhanced the method efficiency. The detection results of *Escherichia coli* (*E. coli*) and *Staphylococcus aureus* (*S. aureus*) under different heating conditions showed that the peak current values of *E. coli* and *S. aureus* were the highest after heating at 50 °C for 15 min. The dynamic changes in the electrochemical signals from the heat-treated bacteria with alteration in heating conditions were indicated to be related to the effects of heating on the external structure and purine metabolism of the bacterial cells. Although heat-treated *E. coli* and *S. aureus* exhibited similar peak potentials, different substances were observed to have contributed to these potentials. A positive linear correlation was observed between the peak current and bacterial concentration. Compared to the plate counting method, the electrochemical method detected the activity changes in *E. coli* and *S. aureus* from the logarithmic to the stationary phase earlier. The findings support the broad application of electrochemical methods in microbial detection and provide valuable insights into the purine metabolism of heat-stressed bacteria.

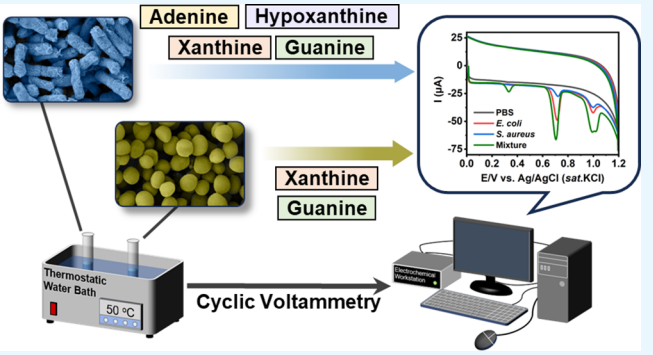

1. INTRODUCTION

Bacterial infections are a leading cause of death globally. A recent study conducted in 2019 analyzed 33 types of bacteria, leaking them to 7.7 million deaths, which represent 13.6% of all global deaths.[1] Therefore, it is imperative to develop effective and reliable methods to monitor and detect pathogenic bacteria. However, most traditional methods, such as microbiological culture, which depend heavily on bacterial multiplication,[2] do not meet accuracy standards. This is because bacterial viability involves complex physiological activities beyond mere proliferation, as further studies of bacterial physiology suggest.[3,4] Molecular biology-based techniques, including enzyme-linked immunosorbent assay (ELISA),[5] polymerase chain reaction (PCR),[6] and deoxyribonucleic acid (DNA) probe,[7] show high sensitivity and selectivity in detecting bacteria. However, these methods necessitate sophisticated instrumentation and skilled professionals due to their complex procedures.

Electrochemistry has emerged as a breakthrough method that overcomes the limitations of existing techniques for detecting microorganisms. Compared to the conventional methods like turbidity measurement and plate counting, electrochemical techniques offer superior efficiency and significantly reduce detection times from hours down to minutes.[8,9] Unlike the techniques based on molecular biology, electrochemical methods require lightweight equipment, are cost-effective, are simple to operate, and maintain high sensitivity and accuracy. The principle underlying electrochemical bacterial detection involves converting bacterial metabolites into electrical signals by using an electrochemical analyzer. This method measures changes in current, resistance, or voltage to indicate the presence and activity of bacteria.[10] Therefore, electrochemistry is widely utilized for tasks such as monitoring microbial growth,[11,12] quantifying microbial concentrations,[13,14] and accessing antimicrobial drugs[15−17] as well as for sterilization and the selective and qualitative detection of bacteria.[18−20] Electrochemistry has also advanced our understanding of the mechanism behind bacterial electron transfer mediated by redox shuttles.[21−23] For instance, Han et al. detected six microorganisms including *Escherichia coli* (*E.*

Received: January 25, 2024
Revised: July 26, 2024
Accepted: October 16, 2024
Published: October 29, 2024

coli), *Bacillus subtilis*, and *Staphylococcus aureus* (*S. aureus*) on a tetracycline-modified glassy carbon electrode (GCE). This study preliminarily inferred that electrochemical reactions are caused by electron mediators within electron-transport chains, such as cytochrome oxidase and cytochrome C.[24] Similarly, You et al. demonstrated how flavins in the culture suspension of isolated Gram-positive *Bacillus megaterium* strain LLD-1 act as effective electron shuttles, enhancing our understanding of extracellular electron transfer mechanisms.[25] In addition, previous studies have shown that phenazine[26,27] and quinone[28,29] secreted by bacteria could also act as mediators of bacterial electron transfer. Wang et al. investigated the electrochemical behavior of *S. aureus* secretion over 2 h using the GCE modified by multiwalled carbon nanotubes (MWCNTs).[30] This study elucidated the electron transfer mechanism by linking electrochemical signals to the oxidation of purine and established a strong linear relationship between the bacterial concentration and peak current. Furthermore, monitoring bacterial growth and evaluating levofloxacin inhibition suggested that this dual-signal electrochemical detection system could become a novel tool for analyzing bacterial vitality. However, there are limitations to consider: the electrically active substances secreted by bacteria must reach a specific concentration to be detectable, a process that can be time-consuming due to their gradual secretion. Additionally, these electroactive substances may vary over time, potentially impacting the precision of the detection process.

Previous studies have reported that the bacterial membrane system exposed to heat stress could exhibit increased permeability, potentially leading to leakage of the intracellular substances.[31,32] For example, Hoffman et al. discovered that heating *E. coli* at 43 °C and above resulted in cell wall expansion.[33] Russell et al. found that the cytoplasmic membrane of *E. coli* was damaged at 50 °C, causing leakage of bacterial internal nucleic acids.[34] Therefore, brief heat treatment of bacteria may significantly enhance the electrochemical response. In the present study, heating was utilized as a pretreatment in the electrochemical detection process to enhance the release of intracellular metabolites, shorten the detection time, and improve the detection efficiency.

MWCNTs are currently regarded as a highly stable and well-researched electrode modification material. Their high surface area renders them ideal for immobilization on the electrode surfaces, facilitating the attachment of additional biosensor receptors. This, in turn, enhances the efficiency of electron transfer on the electrode surface and amplifies the electrical signal.[35−37] The electrochemical behaviors of heat-treated *E. coli* (Gram-positive) and *S. aureus* (Gram-negative) MWCNTs/GCE were extensively studied, focusing on the effects of the heating duration and temperature on the electrochemical signals and their underlying mechanisms. It was observed that changes in the electrochemical signals were closely related to alterations in the external cell structures and purine metabolism. Although both *E. coli* and *S. aureus* exhibited the same electrochemical peak potentials, differences were noted in the substances contributing to the peak currents. The results of bacterial growth monitoring showed that the system had significant potential in reflecting changes in the bacterial activity. The findings of this study may underscore the utility of electrochemical methods in microbial detection and provide detailed insights into the physiological changes that bacteria undergo under heat stress, including associated electron transfer mechanisms.

2. MATERIALS AND METHODS

2.1. Reagents and Chemicals. Sodium chloride, peptone, beef paste, and AGAR powder were obtained from AOBOX Biotech (Beijing, China). Uric acid (UA), xanthine (X), guanine (G), adenine (A), hypoxanthine (HX), and xanthine oxidase (XO) were acquired from Sigma (USA). Multiwalled carbon nanotubes (MWCNTs) were obtained from Shenzhen Nanotech Port Co. (China). 2-Nitrophenyl-β-D-galactopyranoside (ONPG) and *N*-phenyl-1-naphthylamine (NPN) were purchased from Shanghai Aladdin Biochemical Technology Co., Ltd. (China). 4-(2-Hydroxyethyl)-piperazine-1-ethanesulfonic acid (HEPES) was acquired from Shanghai Macklin Biochemical Technology Co., Ltd. (China). Glucose was purchased from Beijing Solarbio Science & Technology Co., Ltd. (China). All other chemicals used were of analytical grade and were used as received.

2.2. Bacterial Cultivation and Sample Preparation. The *S. aureus* (ATCC6538) and *E. coli* (ATCC8739) strains were revived through overnight incubation at 37 °C in a broth medium. The strains were inoculated in 150 mL of the broth medium and incubated overnight at 37 °C with shaking. Cells in the logarithmic growth phase (for both *E. coli* and *S. aureus*) were harvested by centrifugation at 6000 rpm for 15 min, washed, and resuspended in PBS. The bacterial suspension was heated in a water bath and then centrifuged at 6000 rpm for 15 min. The resulting supernatant was used as the test sample.

2.3. Preparation of MWCNTs/GCE and Electrochemical Detection. The GCE (3 mm diameter, Wuhan Gaoshi Ruilian Technology Co., Ltd., China) was polished and ultrasonically cleaned in triple-distilled water followed by ethanol. Subsequently, the GCE was coated with 6 μL of a 2 mg/mL MWCNT suspension and dried to obtain the MWCNTs/GCE. Electrochemical detection was conducted using a CHI615 electrochemical workstation (Shanghai Chenhua Apparatus Co., China). A three-electrode system was employed, consisting of MWCNTs/GCE as the working electrode, Ag/AgCl (saturated KCl, Wuhan Gaoshi Ruilian Technology Co., China) as the reference electrode, and a platinum wire (Wuhan Gaoshi Ruilian Technology Co., China) as the counter electrode. Cyclic voltammetry (CV) was performed over a potential range of 0−1.2 V.

2.4. Attribution of Electrochemical Signals. The preliminary attribution of electrochemical signals was achieved by electrochemical detection. First, the CV behavior of 5 μmol/L UA, X, G, A, and HX, and their mixtures, was detected and compared to complete the identification of the signal peak sources from the mixture. Subsequently, the CV profiles of the test sample and the mixture were compared to tentatively determine the electrochemical signal source from heat-stressed bacteria.

The origins of the electrochemical signal peaks were further determined by using high performance liquid chromatography (HPLC). HPLC chromatograms for a mixed standard of UA, X, G, A, and HX were compared against individual standards to determine the retention time of each substance. By comparison of the retention time of chromatographic peaks between the test samples and the mixed standard, the sources of the electrochemically active substances were identified. HPLC analyses were performed using a model e2695 HPLC system (Thermo Fisher Scientific Inc., USA) at 254 nm,

https://doi.org/10.1021/acsomega.4c00756
ACS Omega 2024, 9, 44907−44915

equipped with an Agilent 1100 separation module comprising an Ascenis RP-Amide column (250 mm × 4.6 mm, ID 5.0 μm) at 25 °C. The mobile phase, consisting of 0.047 mmol/L KH_2PO_4 (pH = 4), was run at a rate of 1.0 mL/min. Each injection into the HPLC system was 20 μL. Both the standards and test samples were filtered through 0.22 μm microporous filters before analysis.

The enzyme-catalyzed electrochemical method was used for further accurate attribution of the detected electrochemical signals. XO, the rate-limiting enzyme in the purine degradation process, oxidizes HX into X and subsequently X into UA. Comparing the electrochemical behaviors before and after adding XO to the samples and mixed standards revealed the specific substances responsible for the electrochemical signal peaks. Following the CV detection of purine standards and bacterial supernatant, 10 μL of diluted XO was added followed by incubation at 37 °C for 10 min. The CV detection was then carried out.

2.5. External Morphology Observation of Heat-Stressed *E. coli* and *S. aureus*. *E. coli* and *S. aureus* cells in the logarithmic growth phase were collected through centrifugation, washed twice, and then suspended in PBS. Subsequently, the bacterial suspension was heated in a water bath. The bacterial sediment was obtained through centrifugation and fixed at 4 °C for 4 h using a fixative solution of paraformaldehyde−glutaraldehyde (2/2.5%, Shanghai, China) and dehydration using an ethanol gradient. After being dried, the collected bacterial powder was affixed to conductive tape and subsequently coated with a uniform spray of gold particles. The bacterial morphology was examined using a GeminiSEM 360 field emission SEM instrument (Carl Zeiss Co., Ltd., Germany).

2.6. Permeability Detection of the Bacterial Cell Membrane and Cell Wall. The disruption of the bacterial cell membrane and cell wall can lead to the leakage of intracellular macromolecules. A BCA protein concentration assay kit (Boster Biological Technology Co., Ltd., Wuhan, China) was used to quantify the protein concentrations in the test sample. The protein leakage amount was indicated by the absorbance of the bacterial supernatant at 562 nm.[38]

The permeability of the inner membrane was measured using the ONPG method.[39] β-Galactosidase, an enzyme in the inner membrane of bacterial cells, converts the substrate ONPG into a colored product known as *o*-nitrophenol (ONP). The absorbance of the ONP serves as a measure of the bacterial inner membrane permeability. In this study, 30 mmol/L ONPG was added to the bacterial supernatant and incubated at 37 °C for 3 h. Subsequently, the permeability of the bacterial inner membrane was determined by measuring the absorbance at 415 nm.

NPN was used to detect the permeability of the *E. coli* outer membrane.[40] NPN, a hydrophobic probe, is commonly used to assess the integrity of the bacterial outer membrane. When the outer membrane is compromised, the exposed phospholipid layer allows the NPN to bind. This binding induces blue fluorescence upon excitation at a specific wavelength. The intensity of this fluorescence quantifies the extent of damage to the outer membrane. A sediment of *E. coli* in the logarithmic growth phase was collected via centrifugation, washed twice, and then suspended in HEPES and glucose buffer. After heating, the suspension was cooled in an ice bath before adding 30 μmol/L NPN. Fluorescence intensity was measured using a Fluoroskan Ascent FL fluorescence and chemiluminescence microplate reader (Thermo Fisher Scientific Inc., USA) at excitation and emission wavelengths of 350 and 420 nm, respectively.

Alkaline phosphatase (AKP), located between the bacterial cell membrane and cell wall, provides valuable insights into the integrity of the bacterial cell wall due to its presence and activity.[41] Therefore, the bacterial supernatant was collected and analyzed using an AKP kit (Beyotime Biotechnology, Shanghai, China), and the absorbance was measured at a wavelength of 405 nm. AKP activity in the samples was calculated based on the definition of diethanolamine (DEA) enzyme activity.

2.7. Detection of Purine Leakage. The purine content was measured using HPLC by first analyzing purine standards at various concentrations to establish a linear relationship between the concentration and chromatographic peak area. Subsequently, the chromatographic peak area of each purine in the samples was used to calculate the purine content via corresponding linear equations. All standards and test samples were filtered through 0.22 μm microporous filters before analysis.

2.8. Description of the Growth Curve of *E. coli* and *S. aureus*. The *E. coli* and *S. aureus* cells were cultured, inoculated at 10% into a fresh broth medium, and then transferred into 11 test tubes for further culturing at 37 °C. CV and plate counting were performed at 0, 1, 2, 4, 6, 8, 10, 12, 24, 28, and 32 h.

3. RESULTS AND DISCUSSION

3.1. Repeatability, Reproducibility, Stability, and Anti-Interference Ability of MWCNTs/GCE. The repeatability of MWCNTs/GCE was evaluated by continuously measuring the 1×10^{-3} μmol/L G standard solution. The relative standard deviation (RSD) of 27 consecutive measurements was 3.83%, demonstrating that MWCNTs/GCE could be used for continuous measurements in subsequent research (Figure S1A). Subsequently, five parallel MWCNTs/GCE samples were used for detecting the G standard solution, yielding an RSD of 1.79% in peak current, which indicated excellent reproducibility (Figure S1B). Additionally, when the MWCNTs/GCE electrode was stored in PBS (pH 7.4) at 4 °C, the peak current of the guanine standard solution measured after 48 h was 96.1% of the initial current, decreasing slightly to 92.3% after 5 days. This consistent performance over time suggests that MWCNTs/GCE maintains stability under these conditions. To assess the anti-interference resistance of the electrode, organic and inorganic substances potentially present in the bacterial samples were added to a 5 μmol/L mixed standard solution. The relative errors in the peak current intensity caused by interfering substances were within ±10% each, indicating minimal interference with the electrochemical detection (Table S1). This finding underscores the good selectivity of MWCNTs/GCE toward purine. Furthermore, good recoveries obtained using spiked samples also confirmed the reliability of MWCNTs/GCE (Table S2).

3.2. CV Behavior of Heat-Stressed *E. coli* and *S. aureus*. The CV behavior of samples on the bare GCE and MWCNTs/GCE was investigated. The CV curve for MWCNTs/GCE in PBS (pH 7.4) was smooth, showing no signal peaks and indicating that PBS (pH 7.4) as a blank solution had no impact on the electrochemical detection. In addition, the electrochemical response of heat-treated *E. coli* and *S. aureus* on MWCNTs/GCE was significantly stronger

https://doi.org/10.1021/acsomega.4c00756
ACS Omega 2024, 9, 44907−44915

than on the bare GCE, suggesting that MWCNTs effectively accelerated electron transfer (Figure 1). For both heat-stressed

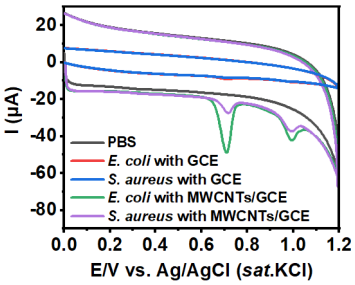

Figure 1. CV behavior of heat-treated *E. coli* and *S. aureus* on the bare GCE and MWCNTs/GCE.

E. coli and *S. aureus*, two stable and significant electrochemical signals were observed on MWCNTs/GCE, with no reduction peaks detected upon reverse scanning, indicating irreversible electrochemical reactions (Figure 1). For heat-stressed *E. coli*, two distinct oxidation peaks were obtained at +0.71 V (signal 1) and +1.01 V (signal 2). Similarly, the CV curve for heat-stressed *S. aureus* also had two distinct oxidation peaks at +0.70 V (signal 1) and +0.97 V (signal 2).

3.3. Attribution of Electrochemical Signals. The electrochemical behaviors of both monomers and a mixture of purine standards were compared (Figure S2). Signal 1 was consistent with the signals of X and G, while signal 2 corresponded to those from HX and A (Figure 2A). The analysis of HPLC demonstrated that heat-stressed *E. coli* contained G, X, HX, and A, whereas heat-stressed *S. aureus* contained only G and A (Figure 2B). Given that XO catalyzes

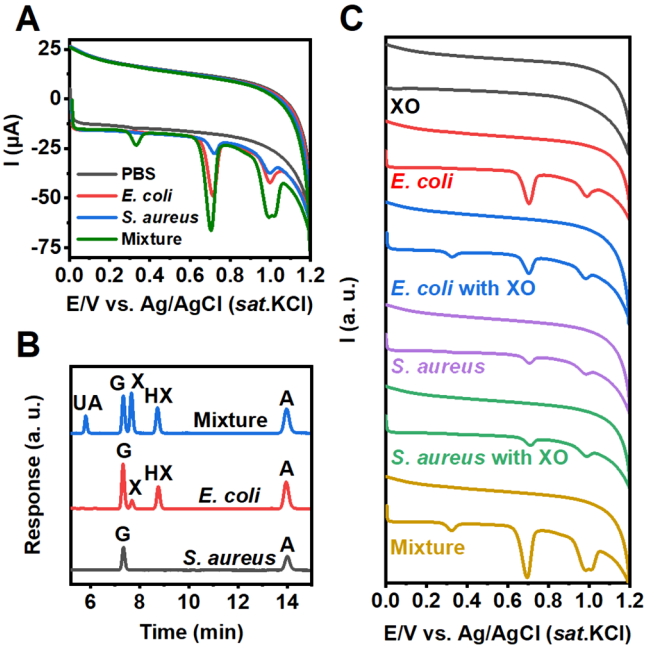

Figure 2. (A) CV of PBS, heated *E. coli*, heated *S. aureus*, and a mixture of standards on MWCNTs/GCE. (B) HPLC of heated *E. coli* and *S. aureus* and mixture. (C) CV of the supernatant from the mixture, heated *E. coli*, and heated *S. aureus* before and after adding XO. XO: xanthine oxidase, HX: hypoxanthine, X: xanthine, A: adenine, G: guanine, UA: uric acid. Mixture: mixture of UA, X, G, HX, and A. Heating temperature: 50 °C. Heating time: 15 min.

the conversion of X and HX into UA, observing changes in electrochemical response before and after adding XO could be crucial for further identification. The reduction of signal 1 and signal 2 in *E. coli* and the appearance of a new peak at around +0.3 V after adding XO implied that signal 1 of heat-stressed *E. coli* was due to X and G and signal 2 to HX and A (Figure 2C). However, the electrochemical responses of heat-stressed *S. aureus* remained unchanged after adding XO, indicating that signal 1 and signal 2 originated from G and A, respectively (Figure 2C). This finding aligned with the CV and HPLC for unheated *S. aureus* reported by Wang et al.[30] Therefore, it was concluded that the substances causing electrical activity differed, although heated *E. coli* and *S. aureus* exhibited similar peaks at potentials around +0.7 and +1.0 V, respectively.

3.4. Dynamic Changes in Electrochemical Responses of Heat-Stressed *E. coli* and *S. aureus*. To optimize heating conditions, dynamic changes in electrochemical signals on MWCNTs/GCE for *E. coli* and *S. aureus* were investigated across various durations and temperatures. For *E. coli*, as the temperature increased, the peak currents of the two signals initially rose, peaking at 50 °C before decline. At 70 and 80 °C, no significant differences were observed in the two signals, indicating that higher temperatures do not enhance the electrochemical responses. The peak currents from *E. coli* heated at 50 °C were significantly higher than those from unheated bacteria, remaining stable from 15 min for both signals (Figure 3A,B). Similarly, for *S. aureus*, peak currents at

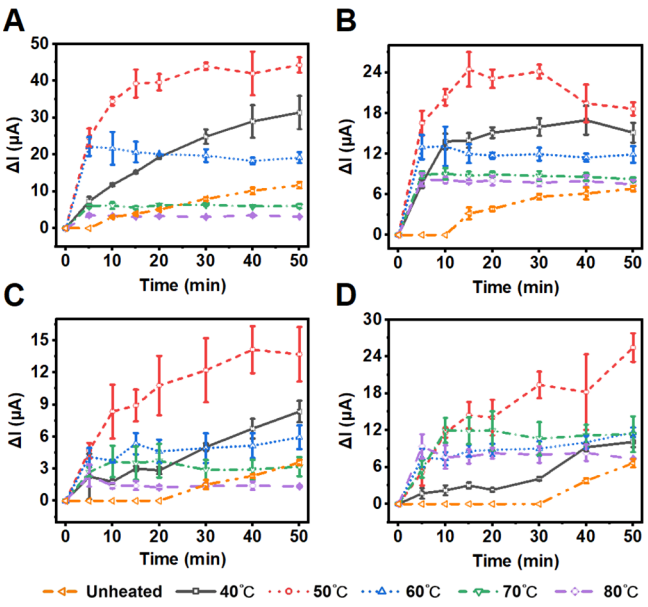

Figure 3. (A, B) Changes in peak current of (A) signal 1 and (B) signal 2 from heat-stressed *E. coli*. (C, D) Changes in peak current of (C) signal 1 and (D) signal 2 from heat-stressed *S. aureus*. Heating times: 0, 5, 10, 15, 20, 30, 40, and 50 min.

50 °C are higher than those at other temperatures, mirroring the phenomenon observed in *E. coli* (Figure 3C,D). Additionally, at 40 and 50 °C, the rise in *S. aureus* peak currents lagged behind *E. coli*, reaching maximum values after a longer duration. This lag may be attributed to the greater robustness of the *S. aureus* membrane system. The results clearly demonstrate the heat's crucial role as a pretreatment in electrochemistry, significantly enhancing peak currents, with varying conditions producing distinct outcomes.

https://doi.org/10.1021/acsomega.4c00756
ACS Omega 2024, 9, 44907−44915

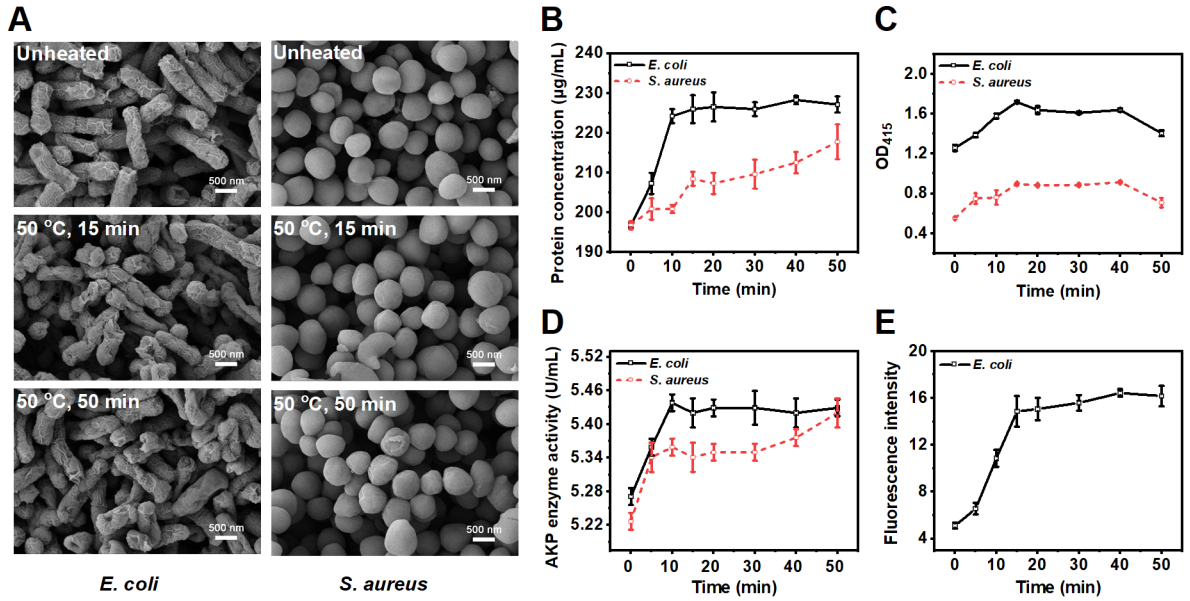

Figure 4. (A) SEM of *E. coli* and *S. aureus* treated with different heating conditions. Magnification was 20,000×. (B–D) Changes in the (B) protein concentration, (C) OD_{415}, and (D) AKP enzyme activity of heat-stressed *E. coli* and *S. aureus*. (E) Changes in fluorescence intensity of heat-stressed *E. coli*. Heating temperature: 50 °C. Heating times: 0, 5, 10, 15, 20, 30, 40, and 50 min.

3.5. Changes in Morphology and Permeability of the External Structure of Heat-Stressed *E. coli* and *S. aureus*. Heat stress directly affects the morphology and permeability of the bacterial external structure, which includes the inner membrane, outer membrane, and cell wall.[42]

The morphologies of heat-stressed *E. coli* and *S. aureus* were examined by using SEM (Figure 4A). Unheated *E. coli* exhibited a regular and short rod shape. After 15 min of heat treatment, its morphology became distorted and deformed, featuring a shrunken and rough surface along with some cavities. Fractures developed after 50 min of heating. No evident changes were observed in the morphology of *S. aureus* after increasing the heating duration from 15 to 50 min, indicating greater heat resistance.

Membrane damage was assessed by evaluating protein leaked into the supernatant. Heating did not aggravate membrane damage in *E. coli* after 10 min. Protein leakage in *S. aureus* increased at two points compared to *E. coli*, implying that the prolonged heating disrupted membrane permeability balance, possibly maintained by a regulatory mechanism against heat stress (Figure 4B). *β*-Galactosidase leakage analysis revealed rapid increases in inner membrane permeability for both *E. coli* and *S. aureus* upon heating within a short duration (Figure 4C). The decreased *β*-galactosidase levels could be attributed to its denaturation. The extracellular AKP levels in *E. coli* exhibited no significant increase after 10 min of heating. In contrast, the AKP leakage in *S. aureus* showed a delayed increase after 30 min, possibly due to its thicker cell wall (Figure 4D).

The effect of heating on the outer membrane, a characteristic structure of Gram-negative bacteria, was examined (Figure 4E). The stability of fluorescence intensity at 15 min suggested that the heat's impact on the outer membrane of *E. coli* peaked at this time, coinciding with the stabilization of the peak current.

Given the evidence, it was inferred that the changes in the external structures of *E. coli* and *S. aureus* upon heat treatment varied, with the latter exhibiting greater heat resistance. However, while similarities were observed in their response patterns to heating, it remains unclear whether the dynamic changes in peak currents primarily result from the varying permeability of the external structure.

3.6. Effects of Heat Stress on Purine Released by *E. coli* and *S. aureus*. Using HPLC, we determined the concentrations of purines released by *E. coli* and *S. aureus* during heating at 50 °C. For the heat-treated *E. coli* samples, the concentration of X increased with the duration of heating. The level of HX decreased sharply after 5 min and then gradually stabilized. Concentrations of G and A rose significantly until 15 min and decreased after 30 min (Figure 5A). These results indicate that the initial rapid increase in the

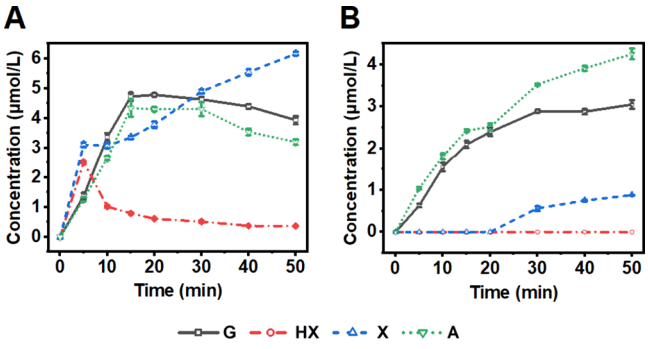

Figure 5. Concentration of purine released by heat-treated (A) *E. coli* and (B) *S. aureus*. Heating temperature: 50 °C. Heating times: 0, 5, 10, 15, 20, 30, 40, and 50 min.

E. coli signal 1 within 15 min results from concurrent rises in X and G, while the post-15 min stability of this signal arises from the ongoing increase in X and the reduction of G. Signal 2 for *E. coli* remained stable after 15 min, reflecting the changes in A and HX. In parallel, the purine profiles in *S. aureus* samples also varied with heating time. The concentration of G notably increased within the first 30 min and then stabilized. Conversely, the concentration of A continuously increased

https://doi.org/10.1021/acsomega.4c00756
ACS Omega 2024, 9, 44907−44915

throughout the heating process. X was not detected until 30 min, after which it started to increase. No HX was detected during the entire heating period (Figure 5B). These variations suggest that the increases in signal 1 of *S. aureus* before 30 min are primarily due to G, while after 30 min, they result from combined increases in X and G. The changes in signal 2 are attributed solely to A. These findings demonstrate that heating time significantly influences the purine content, thereby affecting the composition of electrochemical signal contributions at this temperature.

These changes may be linked to various enzymes involved in purine biosynthesis, salvage, and interaction including purine nucleoside phosphorylase and phosphoribosyltransferase.[43,44] Initially, it was hypothesized that after 5 min, the accumulation of X and the decline of HX in *E. coli* were due to the heightened activity of xanthine dehydrogenase (XHD), which catalyzes the oxidation of HX into X and then X to UA (Figure 5A). However, despite references to the optimal culture temperature and the absence of UA, the lack of studies on the thermostability of XHD released from *E. coli* or *S. aureus* does not fully explain the observed changes. Therefore, it was considered that heat might promote the branch reaction from inosine monophosphate (IMP) to guanosine monophosphate (GMP) through specific mechanisms.[45] The similar trends in the concentrations of G and A in *E. coli* during heating suggested that the same enzyme, possibly purine nucleoside phosphorylase, might facilitate the interconversion of these purine nucleosides (Figure 5A). The concentrations of G and A in *S. aureus* exhibited similar trends with increasing heating time. Unlike *E. coli*, these concentrations of G and A in *S. aureus* remained steady or even increased in the later stages of heating (Figure 5B). In addition, there was no HX in the *S. aureus* heat treatment solution. These findings might have been attributed to differences in purine metabolism between *E. coli* and *S. aureus*.

Heat-induced damage to cell structures can significantly influence the permeability and variation in the purine content. In *E. coli*, both cell structure permeability and purine content increase rapidly during the initial phase of short-term heating. Permeability then stabilizes during the mid to late stages, while the purine content continues to change. This pattern suggests that early heating disrupts *E. coli* structural integrity, causing a swift release of purine accumulated within the cells. As the heating extends, further damage worsens, but once the maximum damage is reached, permeability plateaus. At this stage, changes in purine levels are primarily driven by heat-altered metabolic and transformation pathways within the maximum limits of permeability. For *S. aureus*, which exhibits greater heat tolerance than *E. coli*, initial heat stress rapidly increases both permeability and purine leakage due to cell structure damage. As heating continues, *S. aureus* likely activates regulatory mechanisms that accelerate the synthesis of structural components, although repair processes for membrane and cell wall damage do not occur synchronously.[46] This asynchrony results in varying rates of permeability changes, with gradual increases in the leakage of A and G within the established limits of permeability. Beyond 30 min, the repair rate lags behind the damage rate caused by heating, markedly increasing permeability and possibly enhancing A leakage due to the direct impact of heat on A metabolism. Meanwhile, the stability of the G concentration might be predominantly due to metabolic adjustments rather than structural changes. Notably, the absence of X detection during cell damage and repair phases implies no initial accumulation within the cells, suggesting that prolonged heating may stimulate X generation, increasing its leakage. These observations underscore that the release of purine during heating is a complex interplay of cell structure permeability and metabolic changes. This preliminary hypothesis highlights the need for further investigation into the mechanisms driving these changes in bacterial electrochemical responses and purine metabolism upon heating utilizing molecular biology and other advanced techniques.

3.7. Effects of Electrochemical Detection Parameters on Electrochemical Signals. The peak currents for signal 1 of *E. coli* and both signals from *S. aureus* peaked when the acidity of PBS was 7.4; however, this acidity did not significantly affect signal 2 of *E. coli* (Figure S5). A decrease in acidity led to a negative shift in the peak potentials for four signals, suggesting involvement of hydrogen protons in the electrochemical reactions. Furthermore, the signal potentials exhibited strong linear relationships with pH (Figure 6A,B).

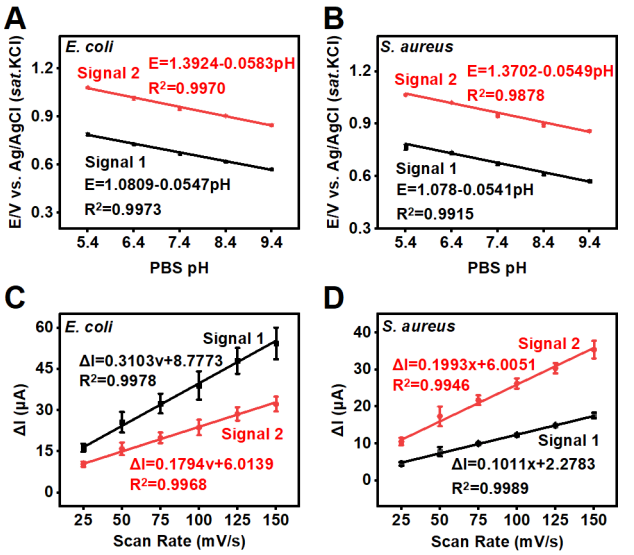

Figure 6. (A, B) Peak current of heat-stressed (A) *E. coli* and (B) *S. aureus* with different acidities. (C, D) Linear relationships between scan rate and peak current of heat-stressed (C) *E. coli* and (D) *S. aureus*.

The slope of each equation approached a theoretical value of 0.0592 V/pH, as per the Nernst equation, suggesting that the oxidation reactions for *E. coli* and *S. aureus* signals were isoelectronic and isoprotonic. Consequently, a pH of 7.4 was selected as the optimal PBS parameter for the electrochemical determination system.

To clarify the oxidation mechanism, the electrochemical behaviors of heat-treated bacteria were investigated at various scan rates. For both *E. coli* and *S. aureus*, strong linear relationships between the peak currents of the signals and the scan rate indicated that the electrochemical reactions were controlled by adsorption (Figure 6C,D). Moreover, the effects of enrichment time and potentials on the peak currents of *E. coli* and *S. aureus* were studied (Figures S6 and S7). Accordingly, 360 s and 0 V were identified as the optimal enrichment times and potential for future electrochemical experiments.

3.8. Relationships between the Electrochemical Signals of Heat-Stressed *E. coli* and *S. aureus* and

https://doi.org/10.1021/acsomega.4c00756
ACS Omega 2024, 9, 44907−44915

Their Concentrations. The experimental results demonstrated strong linear relationships between the peak currents of the two signals from heat-treated *E. coli* (Figure 7A), heat-treated *S. aureus* (Figure 7B), and their respective concentrations. The detection limits for signal 1 and signal 2 in *E. coli* were 0.866×10^6 and 9.740×10^5 CFU/mL, respectively. For *S. aureus*, the limits were 4.872×10^6 CFU/mL for signal 1 and 1.513×10^6 CFU/mL for signal 2.[47]

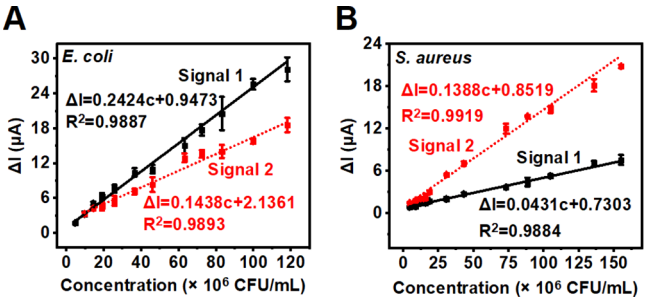

Figure 7. Linear relationships between the peak current and concentration of heat-stressed (A) *E. coli* and (B) *S. aureus*.

3.9. Description of the Growth Curves of *E. coli* and *S. aureus*. Plate counting is a traditional method for generating bacterial growth curves based on the visibility of colonies. This approach depends on the interaction of various bacterial metabolic processes and a suitable external environment, necessitating time for visible colony formation. Consequently, plate counts may reflect the growth stages with some lag. This study compared growth curves derived from electrochemical signals and plate counting to determine if the electrochemical method could detect different phases of bacterial growth earlier. The electrochemical results showed that signals 1 and 2 for *E. coli* increased significantly up to 10 and 6 h, respectively, before the rate of increase slowed and eventually stabilized. This suggested that *E. coli* was in the logarithmic growth phase before 10 h, characterized by active purine metabolism. After 10 h, it transitioned into the stationary phase of metabolism and proliferation (Figure 8A). Signal 2 indicated a notable decrease at 32 h, marking the onset of declining metabolic activity and entry into the apoptotic phase. In contrast, plate counting indicated that *E. coli* proliferated rapidly before 12 h and then entered the stationary phase, which was detected later than the electrochemical method. Similarly, the electrochemical signal 2 for *S. aureus* stabilized from 6 h onward, suggesting an early entry into the stationary phase, while plate counting showed no significant change until after 12 h (Figure 8B). These results demonstrate that the electrochemical method could detect transitions from the logarithmic to stationary phases earlier than plate counting. This indicates that the electrochemical responses of heat-treated bacteria hold significant potential for development into a system that can more accurately reflect their proliferation and metabolic activities.

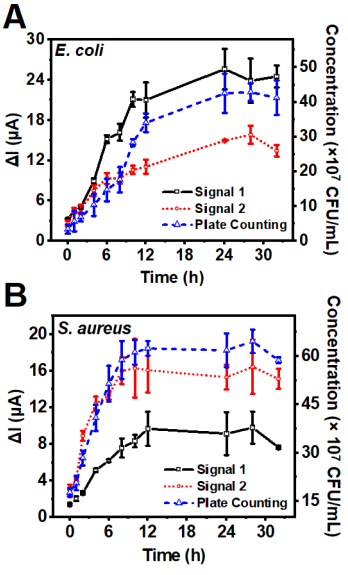

Figure 8. Growth curves of (A) *E. coli* and (B) *S. aureus* described by the plate counting method and electrochemical method.

4. CONCLUSIONS

This study investigated the electrochemical behavior and underlying mechanisms of electrochemical signals from heat-treated bacteria on MWCNTs/GCE and preliminarily established an electrochemical detection method using heat treatment as a pretreatment step. The study found that the peak currents of heat-treated *E. coli* and *S. aureus* were highest after heating at 50 °C for 15 min. For heat-treated *E. coli*, the oxidation peak near +0.70 V was attributed to G and X, and the peak near +1.00 V was attributed to HX and A. For *S. aureus*, the oxidation peak near +0.70 V was attributed to G, and the peak near +1.00 V was attributed to A. The variations in electrochemical signals between *E. coli* and *S. aureus* may stem from differences in cell structure permeability and purine metabolism under various heating conditions. Peak currents showed a strong linear correlation with the bacterial concentration. The electrochemical method detected activity changes in *E. coli* and *S. aureus* from the logarithmic to stable growth phases earlier than the plate counting method. These findings suggest that the electrochemical detection method for thermally treated bacteria holds significant potential for evolving into a mature system that can reflect bacterial proliferation and metabolic activity. Investigating how heat affects purine release from pathogens has enhanced our understanding of the physiology of heat-stressed bacteria.

While the proposed method showed promising results, there is still significant scope for improvement. Future research could use molecular biology techniques to more precisely decipher the underlying mechanism of the signal responses in a more detailed manner. Addressing the current method's limitations, such as high detection limits and a narrow detection range, is crucial for enhancing its efficacy. Utilizing more sensitive electrochemical detection methods such as square wave voltammetry (SWV) or differential pulse voltammetry (DPV) could help overcome these challenges. Exploring electrode modifications with suitable materials could enhance performance, increase sensitivity, and lower detection limits. Miniaturizing the heating device could also enhance the practicality. The successful implementation of the proposed method to *E. coli* and *S. aureus* also indicates its potential extension to other strains, demonstrating broader applicability in microbiological analysis. Further research and validation are needed to confirm the method's effectiveness across a wider range of microorganisms, potentially revolutionizing microbiological testing. With ongoing research and refinement, this method holds great potential to excel in microbiological analysis.

https://doi.org/10.1021/acsomega.4c00756
ACS Omega 2024, 9, 44907−44915

■ ASSOCIATED CONTENT

Supporting Information

The Supporting Information is available free of charge at https://pubs.acs.org/doi/10.1021/acsomega.4c00756.

The detection performance of MWCNTs/GCE; peak attribution of purine electrochemical response; HPLC of purine; effects of PBS pH, enrichment time, and enrichment potentials on peak current of heat-treated *E. coli* and *S. aureus* (PDF)

■ AUTHOR INFORMATION

Corresponding Author

Yanli Zhao − *College of Chemistry and Pharmacy and Heilongjiang Provincial Key Laboratory of New Drug Development and Pharmacotoxicological Evaluation, College of Pharmacy, Jiamusi University, Jiamusi 154007, China*; Email: zhaoyanli@jmsu.edu.cn

Authors

Xiaofan Wu − *College of Chemistry and Pharmacy, Jiamusi University, Jiamusi 154007, China*; orcid.org/0009-0000-5604-3278

Yupo He − *College of Chemistry and Pharmacy, Jiamusi University, Jiamusi 154007, China*

Jiaqi Fu − *College of Chemistry and Pharmacy and Heilongjiang Provincial Key Laboratory of New Drug Development and Pharmacotoxicological Evaluation, College of Pharmacy, Jiamusi University, Jiamusi 154007, China*

Complete contact information is available at: https://pubs.acs.org/10.1021/acsomega.4c00756

Author Contributions

All authors have given approval to the final version of the manuscript.

Notes

The authors declare no competing financial interest.

■ ACKNOWLEDGMENTS

This work was supported by Joint Guidance Project of Natural Science Foundation of Heilongjiang Province (LH2019H058), Heilongjiang Provincial Key Laboratory of New Drug Development, and Pharmacotoxicological Evaluation Project (kfkt2022-07).

■ REFERENCES

(1) GBD 2019 Antimicrobial Resistance Collaborators. Global mortality associated with 33 bacterial pathogens in 2019: a systematic analysis for the Global Burden of Disease Study 2019. *Lancet* **2022**, *400* (10369), 2221−2248.

(2) Wu, E. H.; Yi, J.; Liu, B. H.; Qiao, L. Assessment of bacterial viability by laser desorption ionization mass spectrometry for antimicrobial susceptibility testing. *Talanta* **2021**, *233*, No. 122535.

(3) Wang, M.; Bai, Z. Y.; Liu, S. Y.; Liu, Y. Y.; Wang, Z. Q.; Zhou, G. P.; Gong, X. Y.; Jiang, Y.; Sui, Z. W. Accurate quantification of total bacteria in raw milk by flow cytometry using membrane potential as a key viability parameter. *LWT-Food Sci. Technol.* **2023**, *173*, No. 114315.

(4) Boyte, M.-E.; Benkowski, A.; Pane, M.; Shehata, H. R. Probiotic and postbiotic analytical methods: a perspective of available enumeration techniques. *Front. Microbiol.* **2023**, *14*, No. 1304621.

(5) Zhao, Q.; Lu, D.; Zhang, G. Y.; Zhang, D.; Shi, X. B. Recent improvements in enzyme-linked immunosorbent assays based on nanomaterials. *Talanta* **2021**, *223*, No. 121722.

(6) Yang, J.; Zhang, N. N.; Lv, J.; Zhu, P.; Pan, X.; Hu, J. Q. Z.; Wu, W. F.; Li, S.; Li, H. T. Comparing the performance of conventional PCR, RTQ-PCR, and droplet digital PCR assays in detection of Shigella. *Mol. Cell. Probes* **2020**, *51*, No. 101531.

(7) Zhang, J. L.; He, F. J. Mycobacterium tuberculosis piezoelectric sensor based on AuNPs-mediated enzyme assisted signal amplification. *Talanta* **2022**, *236*, No. 122902.

(8) Jiang, F.; Wang, L.; Jin, N.; Yuan, J.; Li, Y.; Lin, J. Magnetic nanobead chain-assisted real-time impedance monitoring using PCB interdigitated electrode for Salmonella detection. *iScience* **2023**, *26* (11), No. 108245.

(9) Bonaldo, S.; Cretaio, E.; Pasqualotto, E.; Scaramuzza, M.; Franchin, L.; Poggi, S.; Paccagnella, A. Screen-Printed Electrochemical Biosensor for the Detection of Bacteriophage of Lactococcus Lactis for Dairy Production. *IEEE Sens. J.* **2023**, *23* (6), 5552−5560.

(10) Xie, R.; Wang, W. Electrochemically measuring metabolic activity of single live microbes. *Trends Analyt. Chem.* **2023**, *166*, No. 117200.

(11) Shaik, S.; Saminathan, A.; Sharma, D.; Krishnaswamy, J. A.; Mahapatra, D. R. Monitoring microbial growth on a microfluidic lab-on-chip with electrochemical impedance spectroscopic technique. *Biomed. Microdevices* **2021**, *23* (2), 26.

(12) Gao, Y.; Ryu, J.; Liu, L.; Choi, S. A Simple, Inexpensive, and Rapid Method to Assess Antibiotic Effectiveness Against Exoelectrogenic Bacteria. *Biosens. Bioelectron.* **2020**, *168*, No. 112518.

(13) Wang, L.; Xue, L.; Guo, R. Y.; Zheng, L. Y.; Wang, S. Y.; Yao, L.; Huo, X. T.; Liu, N.; Liao, M.; Li, Y. B.; Lin, J. H. Combining impedance biosensor with immunomagnetic separation for rapid screening of Salmonella in poultry supply chains. *Poult. Sci.* **2020**, *99* (3), 1606−1614.

(14) Tieu, M.-V.; Pham, D. T.; Le, H. T. N.; Hoang, T. X.; Cho, S. Rapid and Ultrasensitive Detection of Staphylococcus aureus Using a Gold-Interdigitated Single-Wave-Shaped Electrode (Au-ISWE) Electrochemical Biosensor. *BioChip J.* **2023**, *17* (4), 507−516.

(15) Ghorbanpoor, H.; Dizaji, A. N.; Akcakoca, I.; Blair, E. O.; Ozturk, Y.; Hoskisson, P.; Kocagoz, T.; Avci, H.; Corrigan, D. K.; Guzel, F. D. A fully integrated rapid on-chip antibiotic susceptibility test − A case study for Mycobacterium smegmatis. *Sens. Actuators, A* **2022**, *339*, No. 113515.

(16) Miran, W.; Long, X.; Huang, W.; Okamoto, A. Current Production Capability of Drug-Resistant Pathogen Enables Its Rapid Label-Free Detection Applicable to Wastewater-Based Epidemiology. *Microorganisms* **2022**, *10* (2), 472.

(17) Nemr, C. R.; Smith, S. J.; Liu, W.; Mepham, A. H.; Mohamadi, R. M.; Labib, M.; Kelley, S. O. Nanoparticle-Mediated Capture and Electrochemical Detection of Methicillin-Resistant Staphylococcus aureus. *Anal. Chem.* **2019**, *91* (4), 2847−2853.

(18) Zamzami, M.; Alamoudi, S.; Ahmad, A.; Choudhry, H.; Khan, M. I.; Hosawi, S.; Rabbani, G.; Shalaan, E.-S.; Arkook, B. Direct Identification of Label-Free Gram-Negative Bacteria with Bioreceptor-Free Concentric Interdigitated Electrodes. *Biosensors* **2023**, *13* (2), 179.

(19) Lee, I.; So, H.; Kim, J.; Auh, J.-H.; Wall, M. M.; Li, Y.; Ho, K.; Jun, S. Selective Detection of Escherichia coli K12 and Staphylococcus aureus in Mixed Bacterial Communities Using a Single-Walled Carbon Nanotube (SWCNT)-Functionalized Electrochemical Immunosensor with Dielectrophoretic Concentration. *Nanomaterials* **2023**, *13* (6), 985.

(20) Stilman, W.; Campolim Lenzi, M.; Wackers, G.; Deschaume, O.; Yongabi, D.; Mathijssen, G.; Bartic, C.; Gruber, J.; Wübbenhorst, M.; Heyndrickx, M.; Wagner, P. Low Cost, Sensitive Impedance Detection of E. coli Bacteria in Food-Matrix Samples Using Surface-Imprinted Polymers as Whole-Cell Receptors. *Phys. Status Solidi A* **2021**, *219* (23), No. 2100405.

(21) Krige, A.; Ramser, K.; Sjöblom, M.; Christakopoulos, P.; Rova, U.; Kelly, R. M. A New Approach for Evaluating Electron Transfer Dynamics by Using In Situ Resonance Raman Microscopy and Chronoamperometry in Conjunction with a Dynamic Model. *Appl. Environ. Microbiol.* **2020**, *86* (20), No. e01535-20.

(22) Liu, X.; Zhan, J.; Liu, L.; Gan, F. T.; Ye, J.; Nealson, K. H.; Rensing, C.; Zhou, S. G. In Situ Spectroelectrochemical Characterization Reveals Cytochrome-Mediated Electric Syntrophy in Geobacter Coculture. *Environ. Sci. Technol.* **2021**, *55* (14), 10142−10151.
(23) You, L.; Rao, L.; Tian, X.; Wu, R.; Wu, X.; Zhao, F.; Jiang, Y.; Sun, S. Electrochemical in situ FTIR spectroscopy studies directly extracellular electron transfer of Shewanella oneidensis MR-1. *Electrochim. Acta* **2015**, *170*, 131−139.
(24) Han, S.; Li, X.; Guo, G.; Sun, Y.; Yuan, Z. Voltammetric measurement of microorganism populations. *Anal. Chim. Acta* **2000**, *405*, 115−121.
(25) You, L. X.; Liu, L. D.; Xiao, Y.; Dai, Y. F.; Chen, B. L.; Jiang, Y. X.; Zhao, F. Flavins mediate extracellular electron transfer in Gram-positive Bacillus megaterium strain LLD-1. *Bioelectrochemistry* **2018**, *119*, 196−202.
(26) Rabaey, K.; Boon, N.; Höfte, M.; Verstraete, W. Microbial Phenazine Production Enhances Electron Transfer in Biofuel Cells. *Environ. Sci. Technol.* **2005**, *39* (9), 3401−3408.
(27) Rhodes, Z.; Simoska, O.; Dantanarayana, A.; Stevenson, K. J.; Minteer, S. D. Using structure-function relationships to understand the mechanism of phenazine-mediated extracellular electron transfer in Escherichia coli. *iScience* **2021**, *24* (9), No. 103033.
(28) Franza, T.; Gaudu, P. Quinones: more than electron shuttles. *Res. Microbiol.* **2022**, *173*, No. 103953.
(29) Stevens, E. T.; Van Beeck, W.; Blackburn, B.; Tejedor-Sanz, S.; Rasmussen, A. R. M.; Carter, M. E.; Mevers, E.; Ajo-Franklin, C. M.; Marco, M. L. Lactiplantibacillus plantarum uses ecologically relevant, exogenous quinones for extracellular electron transfer. *mBio* **2023**, *14* (6), No. e02234-23.
(30) Wang, Z.; Gao, H. F.; Cui, J. W.; Zhou, S.; Zhao, Y. L.; Ye, C.; Li, J. L.; Wu, D. M. Two-signal electrochemical detection system for evaluation viability of Staphylococcus aureus. *Electrochim. Acta* **2021**, *367*, No. 137258.
(31) Shao, L.; Zou, B.; Zhao, Y.; Sun, Y.; Li, X.; Dai, R. Inactivation effect and action mode of ohmic heating on Staphylococcus aureus in phosphate-buffered saline. *J. Food Saf.* **2023**, *43* (4), No. e13052.
(32) Chen, L.; Liu, Q.; Zhao, X.; Zhang, H.; Pang, X.; Yang, H. Inactivation efficacies of lactic acid and mild heat treatments against Escherichia coli strains in organic broccoli sprouts. *Food Control* **2022**, *133*, No. 108577.
(33) Hoffman, H.; Valdina, J.; Frank, M. E. Effects of High Incubation Temperature Upon the Cell Wall of Escherichia coli. *J. Bacteriol.* **1966**, *91* (4), 1935−1937.
(34) Russell, A. D.; Harries, D. Damage to Escherichia coli on Exposure to Moist Heat. *Appl. Microbiol.* **1968**, *16* (9), 1394−1399.
(35) Kumar, S.; Sidhu, H. K.; Paul, A. K.; Bhardwaj, N.; Thakur, N. S.; Deep, A. Bioengineered multi-walled carbon nanotube (MWCNT) based biosensors and applications thereof. *Sens. Diagn.* **2023**, *2* (6), 1390−1413.
(36) Mohd Nurazzi, N.; Asyraf, M. R. M.; Khalina, A.; Abdullah, N.; Sabaruddin, F. A.; Kamarudin, S. H.; Ahmad, S.; Mahat, A. M.; Lee, C. L.; Aisyah, H. A.; Norrrahim, M. N. F.; Ilyas, R. A.; Harussani, M. M.; Ishak, M. R.; Sapuan, S. M. Fabrication, Functionalization, and Application of Carbon Nanotube-Reinforced Polymer Composite: An Overview. *Polymers* **2021**, *13* (7), 1047.
(37) Rajabathar, J. R.; Periyasami, G.; Alanazi, A. M.; Govindasamy, M.; Arunachalam, P. Review on Carbon Nanotube Varieties for Healthcare Application: Effect of Preparation Methods and Mechanism Insight. *Processes* **2020**, *8* (12), 1654.
(38) Huang, X.; Bao, X.; Liu, Y.; Wang, Z.; Hu, Q. Catechol-Functional Chitosan/Silver Nanoparticle Composite as a Highly Effective Antibacterial Agent with Species-Specific Mechanisms. *Sci. Rep.* **2017**, *7* (1), 1860.
(39) Tenea, G. N.; Lemsaddek, T. Peptide Extracts from Native Lactic Acid Bacteria Generate Ghost Cells and Spheroplasts upon Interaction with Salmonella enterica, as Promising Food Antimicrobials. *BioMed. Res. Int.* **2020**, *2020*, 1−11.
(40) Muheim, C.; Götzke, H.; Eriksson, A. U.; Lindberg, S.; Lauritsen, I.; Nørholm, M. H. H.; Daley, D. O. Increasing the permeability of Escherichia coli using MAC13243. *Sci. Rep.* **2017**, *7* (1), 17629.
(41) Yang, Y. J.; Lin, M. Y.; Feng, S. Y.; Gu, Q.; Chen, Y. C.; Wang, Y. D.; Song, D. F.; Gao, M. Chemical composition, antibacterial activity, and mechanism of action of essential oil from Litsea cubeba against foodborne bacteria. *J. Food Process. Preserv.* **2020**, *44* (9), No. e14724.
(42) Tian, X.; Shao, L.; Yu, Q.; Liu, Y.; Li, X.; Dai, R. Evaluation of structural changes and intracellular substance leakage of Escherichia coli O157:H7 induced by ohmic heating. *J. Appl. Microbiol.* **2019**, *127* (5), 1430−1441.
(43) Liu, M.; Fu, Y.; Gao, W.; Xian, M.; Zhao, G. Highly Efficient Biosynthesis of Hypoxanthine in Escherichia coli and Transcriptome-Based Analysis of the Purine Metabolism. *ACS Synth. Biol.* **2020**, *9* (3), 525−535.
(44) Chua, S. M.; Fraser, J. A. Surveying purine biosynthesis across the domains of life unveils promising drug targets in pathogens. *Immunol. Cell Biol.* **2020**, *98* (10), 819−831.
(45) Deng, A.; Qiu, Q.; Sun, Q.; Chen, Z.; Wang, J.; Zhang, Y.; Liu, S.; Wen, T. In silico-guided metabolic engineering of Bacillus subtilis for efficient biosynthesis of purine nucleosides by blocking the key backflow nodes. *Biotechnol. Biofuels Bioprod.* **2022**, *15* (1), 82.
(46) Zhang, L.; Hou, L.; Zhang, S.; Kou, X.; Li, R.; Wang, S. Mechanism of S. aureus ATCC 25923 in response to heat stress under different water activity and heating rates. *Food Control* **2020**, *108*, No. 106837.
(47) Shabani, A.; Marquette, C. A.; Mandeville, R.; Lawrence, M. F. Carbon microarrays for the direct impedimetric detection of Bacillus anthracis using Gamma phages as probes. *Analyst* **2013**, *138* (5), 1434−1440.

https://doi.org/10.1021/acsomega.4c00756
ACS Omega 2024, 9, 44907−44915